Narrow-Band Fiber-Coupled Single-Photon Source

Guilherme Stein,[1] Vladislav Bushmakin,[1] Yijun Wang (王奕钧),[1] Andreas W. Schell,[2,3,4] and Ilja Gerhardt[1,*]

[1] *3. Physikalisches Institut, Universität Stuttgart and Stuttgart Research Center of Photonic Engineering (SCoPE), Pfaffenwaldring 57, Stuttgart D-70569, Germany*

[2] *CEITEC – Central European Institute of Technology, Brno University of Technology, Brno 612 00, Czech Republic*

[3] *Institut für Festkörperphysik, Leibniz Universität Hannover, Appelstraße 2, Hannover D-30167, Germany*

[4] *Physikalisch-Technische Bundesanstalt, Bundesallee 100, Braunschweig D-38116, Germany*

(Received 17 September 2019; revised manuscript received 4 March 2020; accepted 16 April 2020; published 18 May 2020)

A single-photon source is an essential tool for the emerging field of quantum technologies. Ideally, it should be spectrally compatible with other photonic devices while providing a high flux of narrow-band photons. The single organic dye molecule dibenzanthanthrene under cryogenic conditions possesses the given characteristics and therefore constitutes a prominent single-photon source. Nevertheless, the implementation of such a single-photon source requires a complex experimental setup involving a cryostat with a confocal microscope for the effective collection of the molecular emission. In the approach presented here we use a single emitter coupled directly to the end facet of an optical fiber. This has the potential to transfer a single-photon source based on a quantum emitter from a proof-of-principle type of setup to a scalable "plug-and-play" device. We present successful coupling of a single organic molecule to an optical fiber and record the excitation spectrum, measure the saturation curve, and analyze the contributions of Raman background fluorescence. The single-photon nature is proven by an antibunched autocorrelation recording, which reveals coherent Rabi oscillations.

DOI: 10.1103/PhysRevApplied.13.054042

I. INTRODUCTION

Single-photon sources are believed to be a key ingredient for quantum communication, quantum-information processing, and quantum measurements. The generation of single photons is mostly achieved by two different approaches. The first approach is via a parametric process, which creates a photon pair, where one photon heralds the presence of its partner. Often, these sources are spectrally broad, which hinders efficient interfacing to other quantum systems. Furthermore, such sources suffer from multiphoton contributions under high pump powers. This ultimately limits the number of available photons, since these sources can only be pumped weakly to decrease unwanted contributions. The alternative approach is to use single emitters, such as atoms, ions, quantum dots, defect centers, or two-dimensional materials. Historically, the first discovered solid-state source of single photons were single molecules. Under cryogenic conditions, they simultaneously deliver a high flux and a narrow-band emission, and are therefore a highly promising system for applications in quantum technology.

For a single-photon source to be useful, in most experiments it is necessary to ensure that the photons are generated in a defined spatial mode, ideally matched to the mode of an optical fiber. This allows for convenient fiber coupling to other devices. Also, as in interference experiments, the modal overlap is crucial. A defined mode such as a Gaussian mode is optimal. Therefore, fiber-coupled single-photon sources allow for integration in quantum networks and hence is applicable beyond a restricted lab frame.

Fibers have been used to deliver light to single emitters since their early days [1]. Still, the ideal device would be fiber coupled in both, excitation and detection. This can be implemented by coupling a single emitter to a fiber end facet, which has been successfully demonstrated for nano diamonds [2] and quantum-dot emitters [3]. To perform this efficiently, the fiber's NA needs to be maximized so that light emitted at large angles is also captured and guided through.

An alternative way of coupling the emission of solid-state quantum emitters to the guided modes of a fiber is through coupling to the evanescent field of a tapered fiber. This has been demonstrated with a variety of emitters such as quantum dots [4–7], nitrogen-vacancy centers in diamond [2,8–10], defects in hexagonal boron nitride [11], as

*ilja@quantumlah.org

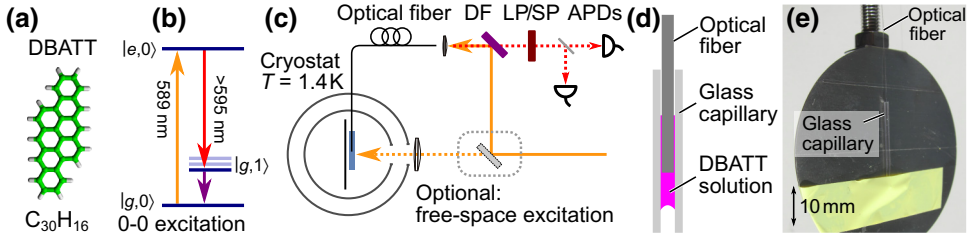

FIG. 1. Experimental configuration. (a) The 2.3,8.9-dibenzanthanthrene (DBATT) molecule used in this study. (b) A simplified level scheme. The resonant zero-phonon-line excitation matches the sodium D_2 transition. (c) In this experiment, a helium bath cryostat hosts the fiber configuration. This setup allows for the excitation through a cryostat window or through the fiber directly. A Hanbury Brown and Twiss configuration allows for the detection of the photon antibunching. DF, dichroic filter; LP and SP, long- and short-pass filter; APDs, avalanche photo diodes. (d) For coupling the molecules, the fiber is inserted in a capillary filled with DBATT solution. (e) The assembly that is cooled down in the cryostat.

well as molecules [12]. Nevertheless, coupling to tapered fibers is difficult as they get contaminated, break, or lose transmission when being cooled down. These problems can be mitigated by directly coupling to a cleaved fiber end facet. Another alternative is the integration of single emitters into waveguides or nanocapillaries [13–17].

The optical properties of single molecules under cryogenic conditions ($T \leq 2\,\mathrm{K}$) are remarkable. One of their advantages is their approximately tenfold larger T_1 time when compared to quantum dots; consequently, their natural linewidth is reduced, and matches other emitters, such as atoms [18,19], which also exhibit lifetimes in the 10-ns range. Coupling to atomic systems can be explored for an efficient storage of the emitted single photons [18]. Furthermore, the amount of spectral diffusion is significantly lower than for other quantum emitters due to their insensitivity against external spin noise, such that Fourier-limited linewidths are commonly observed. Simultaneously, the detected flux of photons reaches up to millions of photons per second while maintaining negligible background contribution.

Here, we present a single-photon source implemented by coupling a single organic molecule to a high NA fiber. This configuration is cooled down to liquid-helium temperatures where the molecules' transitions narrow down to their natural lifetime limit. The optical excitation of the molecules is realized by free-space coupling as well as by direct excitation through the fiber. In both cases the photons are collected and guided towards the detection system by the fiber.

II. EXPERIMENT

Conventional single-mode glass fibers have a numerical aperture around 0.10–0.13. To optimize the collection efficiency, we choose a specialized fiber (UHNA7, Nufern/Coherent Inc.) that is tailored for a wavelength range of 1500–2000 nm and has a core diameter of 2.4 μm, while having a very high numerical aperture of 0.41. In the wavelength range we use in this experiment (600–700 nm), this fiber is not strictly single mode, and changes in the transversal-mode profile are observed when the fiber is bent. The chosen fiber is a compromise between transmission of the fiber and a small core diameter.

The experimental configuration (see Fig. 1) consists of a helium bath cryostat (Janis Inc.) with windows for optical access from the side. The optical fiber is fed into the cryostat through a polytetrafluoroethylene-based seal [20]. The overall length of the fiber is approximately 3 m.

To excite a single molecule, a single-mode dye laser (Coherent 899 dye ring laser, $\Delta\nu \approx 1\,\mathrm{MHz}$) is used. Its linewidth is significantly below the spectral linewidth of the molecules, which enables resonant excitation and measurement of the molecules' transition linewidths. In the fluorescence excitation scheme we use here, the laser excitation at the zero-phonon line is suppressed by the use of a filter (Semrock, LP 593) and only the Stokes-shifted photons are transmitted.

The emitters are 2.3,8.9-dibenzanthanthrene (DBATT) molecules [CAS: 188-42-1, from W. Schmidt, Iggling-Holzhausen, see Fig. 1(a)], which are dissolved in *n*-tetradecane ($C_{14}H_{30}$). The solution is soaked into a glass capillary (a 10–20 mm-long section of a 10-μl pipette, Fa. Hirschmann). Approximately 2 μl of the solution stays inside the capillary. Then the stripped and cleaved optical fiber is inserted into the capillary [see also Fig. 1(d)]. The whole configuration is installed into the cryostat and cooled down to $T = 1.4\,\mathrm{K}$. At cryogenic conditions, the inhomogeneous spectral broadening, caused by different strain and stress on the molecules, spreads their distribution over approximately 1 nm.

Detection is either realized by two free-space single-photon counting modules (SPCM-AQR, Excellitas) in a Hanbury Brown and Twiss configuration or by a compact grating spectrometer (Ocean Optics, QE Pro) for spectrally resolved measurements. The single-photon detection events are captured by a time tagger (Swabian Instruments,

Time Tagger 20). This enables the study of the photon statistics, including antibunching.

III. THEORY

To understand the experimental situation regarding the collection of fluorescent light, other authors use reciprocity theory [21] or numerical methods [22]. However, here we present a more straightforward analytical approach and consider an emitting dipole above an optical fiber; the situation is depicted in Fig. 2(a). To estimate the amount of collected light, both the radiation pattern and the numerical aperture of the fiber have to be considered. The first determines the angular distribution of the molecular emission, while the latter limits its collection to the solid angle formed by the fiber's core.

To describe the radiation pattern, the effect of the dielectric boundaries in the direct proximity of a molecule has to be taken into account. Here we consider the refractive indices of solid *n*-tetradecane and the fiber core given as $n = 1.53$ [23] and $n = 1.501$, respectively. A calculation of the dipolar emission at dielectric interfaces [24] reveals that 19% of the emission of an orthogonal dipole and 33% of the emission of a parallel dipole are emitted into the lower hemisphere, i.e., into the direction of the fiber. Figure 2(a) shows the situation for a dipole located directly at the interface ($h = 0$). The results are shown for an orthogonal dipole (red) and the *r* and *s* components of a parallel-oriented dipole (blue and green).

Figure 2(b) shows the collection efficiency of the fiber for a dipole as a function of its distance from the fiber end facet. In our model, we treat the fiber-core diameter as a capturing region of the molecule's emission with sharp boundaries. Furthermore, we consider a single dipole centered on the optical axis, as any lateral misalignment inevitably leads to a reduction of the coupling efficiency. With this simplified model we show that the numerical aperture sets a strict limit to the maximum collection efficiency into a fiber. In particular, for a parallel dipole with 33% downwards radiation coupling to the given fiber is limited to around 6.1% of its total radiation. This calculation includes interface effects, the numerical aperture and also the geometry of the problem. The latter shows that for larger distances the fibers' NA is not the limiting factor, but the captured solid angle given by the finite size of the fiber core. This limit occurs at a distance of 2.78 μm and beyond. Below this height, the limitations are dominantly imposed by the numerical aperture. We like to note that the redistribution of radiation due to the height of the emitter and the interplay with the optical interface (see above, Ref. [24]) has essentially no influence within the NA-limited collection cone. This is also indicated in Fig. 2(a), where the lobes captured by the numerical aperture resemble the free-space emission dipolar pattern. We attribute this effect

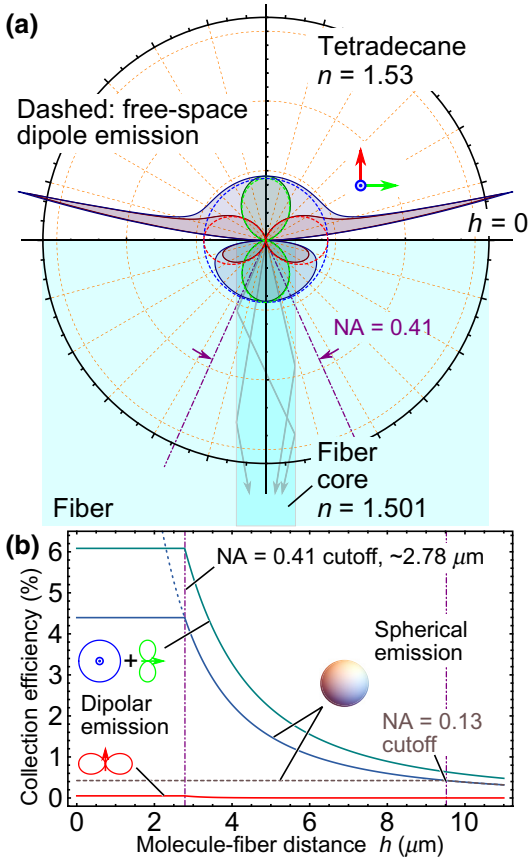

FIG. 2. Collection efficiency of molecular fluorescence into the fiber. (a) Calculated emission pattern of a dipole at a dielectric interface. The refractive indices are given by the molecules' host matrix *n*-tetradecane ($n = 1.53$) and the fiber core of the utilized glass fiber ($n = 1.501$). Therefore, the emission into the upper hemisphere is favored and for a parallel dipole on the interface (projections are shown in blue and green), around two thirds of the emission is emitted upwards. Here the vacuum dipolar emission is depicted by dashed lines, and the emission is calculated with the actual refractive indices as shown by the solid lines. Each color represents a differently oriented dipole. (b) The numerical aperture of the fiber defines a distance, inside which the collection efficiency remains the same. This distance varies for different NAs as shown by the different cutoffs in the graphic. Red and turquoise take the full emission pattern into account, whereas blue and gray show the plots for an assumed spherical emission for comparison. The blue dashed curve indicates radiation of the captured solid angle by the fiber core, which is the same as setting the NA of the fiber to NA = 1. For zero distance, the collection efficiency subsequently corresponds to 50%.

to the lower index of refraction, which is set by the fiber core. If the index difference is reversed, i.e., the fiber's core had the higher refractive index, the redistributed light close to the angle of total internal reflection differs from the simplified description here.

For the situation of an *orthogonal*-oriented dipole [Fig. 2(b), red curve], the collection efficiency is drastically

reduced by a factor of 117. In the case of *spherical* emission [Fig. 2(b), blue curve], there is no influence from the interface and the refractive indices, such that the collection efficiency is solely set by geometrical parameters. The dashed line, which represents the spherical emission in Fig. 2(b), ends for a maximal NA of 1.0, which captures the light in 2π, at a value of 50% collection efficiency for a height of zero (dashed line). We remark that the geometric cutoff is still found to be around a distance of 2.78 μm from the fiber. The distance dependence for spherical emission shows a comparable behavior as the full calculation of the orthogonal oriented dipole. This shows that the dominant part of the orthogonal dipolar emission into the lower hemisphere still behaves proportional to a spherical emission. Since the parallel-oriented dipoles couple better into the fiber core, it implies that the experimental observations of this work are likely based on the detection of parallel-oriented dipoles, which are located within the first few μm above the fiber.

To show how the NA influences the amount of collected light into a commonly used fiber, we consider the single-mode optical fiber 460-HP (Nufern) with a NA of 0.13. We find with this model, that the collection efficiency is limited to below 0.5%. Experiments with such a fiber leads to approximately one order of magnitude less light than with the previously discussed fiber. Due to the lower NA, the corresponding cutoff is around 9.5 μm, i.e., the molecule can be more distant to reach the same effective NA for the collected solid angle. This also implies that the detection volume is increased, leading to a higher background in conjunction with a lower collection efficiency—an unfavorable behavior for our purposes.

We now compare these results to those of a confocal microscope. In our experimental setup we have numerous examples of very high photon flux and record single molecule emission with more than 1.2 million uncorrected detector clicks per second in the past [18,19,25]. These results have been acquired by utilizing a solid immersion lens (SIL) made of cubic zirconia (ZrO_2) with a refractive index of $n = 2.18$, in combination with an aspheric lens with an NA of 0.68 (Geltech, C-330). The overall collection efficiency is calculated as 28%, which is around a factor of 4 to 5 times higher then the calculated value of 6% for the collection with a fiber. Therefore, we estimate the count rate to be a maximum of 250×10^3 counts/s, since the rest of the setup remained the same as in previous experiments. With the reduction of the captured light introduced by spectral filtering (see below), we believe that the results of free-space collection and fiber collection are consistent with each other. Of course, the present collection efficiencies under cryogenic conditions are not comparable to the ideal situation at ambient conditions, where near-unity collection efficiencies can be experimentally reached [26].

IV. RESULTS

To understand the emission of the single molecule and also an eventual background contribution from the fibers, the first task is to record a spectrum of the individual components. This recording is acquired independently from the introduced single-molecule studies in a usual single-molecule experiment (see, e.g., [18,19,27]). The spectra of the light emitted by the molecules and of the background light stemming from the fiber are shown in Fig. 3. It can be clearly seen that both contributions have a substantial spectral overlap: only the higher wavelength sidebands of the molecules are clearly separated from background contributions, which stem from the fiber. Hence, only this part can be effectively separated and used for the single-photon source.

In order to filter out unwanted contributions, spectral filtering is employed. A dichroic long-pass filter (600 nm) is used to suppress the excitation laser light. Unfortunately, this filter suppresses the majority of the Stokes-shifted emission, i.e., $|e,0\rangle \rightarrow |g,1\rangle$. The spectral distance to this band is 241 cm^{-1} from the excitation laser [19]. Still, this filtering is insufficient to account for the remaining background light, which is caused by scattering in the fiber. Therefore, an additional long-pass with cut on at 626 nm is introduced. In order to suppress higher wavelength contributions of the fiber background, an additional short-pass filter with cut on at 678 nm is used. The remaining detection window (626–678 nm) contains only about 30% of the Stokes-shifted photons [28]. This reduces the amount of fluorescence photons, but increases the signal-to-background ratio.

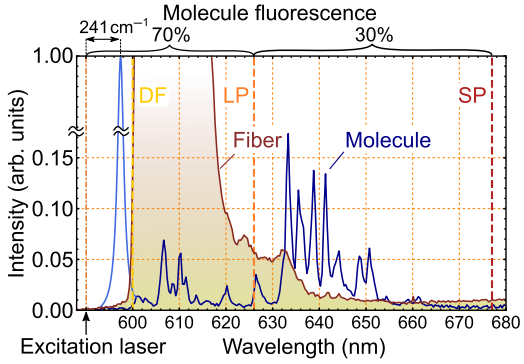

FIG. 3. Spectral contributions of the experiment. The optical fiber exhibits a large amount of background contributions until approximately 630 nm (dark red line). Unfortunately, this overlays the majority (about 70%) of the molecular emission spectrum (blue line). In order to remove these unwanted contributions, a long-pass filter around 630 nm has been introduced (LP). Another background contribution of the fiber is above 700 nm, such that a short-pass filter has also been introduced (SP). To note: we use a dichroic filter (DF) with a sharp cut on around 600 nm. Therefore, the spectra are only recorded from there onwards.

The setup can be operated in two configurations: either by free-space excitation through the cryostat windows or through the fiber. In the first experiment, we employ free-space excitation to reduce the amount of background signal from the fiber. A large focal volume is caused by the $f = 100$-mm lens, which focuses the excitation light to a spot of around 10–20 μm at the fiber tip. The alignment procedure is outlined below. Although we reduce the fiber-induced background, which stems from scattered excitation light, the molecular fluorescence background is increased due to a larger illuminated volume.

To enable the free-space excitation at the fiber tip, several mW of excitation light are used, and all filters in front of the single-photon detectors are removed. Simply, the scattered light, which leaks into the fiber, is sufficient to locate the fiber tip. Therefore, the focus is laterally scanned across the fiber capillary [beam-scanning optics not shown in Fig. 1(e)]. When the fiber end is located, single-molecule detection is attempted. For this, the filters are reinstalled, the excitation laser power is reduced to 200–1000 nW and the laser frequency is scanned through the inhomogeneously broadened band of the molecules around the sodium D-lines. With this scheme, we excite the molecules in their zero-phonon line (ZPL) and subsequently detect only Stokes-shifted photons. When the excitation laser drives the transition in the zero-phonon line from $|g,0\rangle$ to $|e,0\rangle$, the molecule emits approximately 50% of the generated photons into the manifold from $|e,0\rangle$ to $|g,n\rangle$. The other 50% are emitted on the zero-phonon transition [see level scheme in Fig. 1(b)]. Such a ZPL-fluorescence excitation spectrum is shown in Fig. 4(a). As reported before [19], the observed linewidth corresponds to the emission linewidth of a molecule, when a different excitation scheme is implemented. Then, spectral filtering can be implemented by an atomic sodium filter [29,30]. With a spectral linewidth of 62 MHz, this particular molecule exceeds the typical linewidth of single DBATT molecules by a factor of 4–5 [19]. Furthermore, the background contribution is large and the signal-to-background ratio is limited to 2, such that a single-photon recording is not applicable. As commonly observed in single-molecule studies, an increase of the laser power does not lead to an enhanced signal-to-background ratio.

To further explore the technical possibilities, i.e., to excite a single molecule without the full cryostat setup, we now change to an excitation through the optical fiber directly. All alignment steps, except the fiber coupling, can be omitted. The excitation of a molecule is shown in Fig. 4(b). While the linewidth is reduced by a factor of 2, the signal-to-background ratio is approximately the same. Unlike in the case of free-space excitation, we attribute the background to a Raman contribution, which appears to be significant. Although the illuminated sample volume is reduced, we do not observe a significantly better signal-to-background ratio.

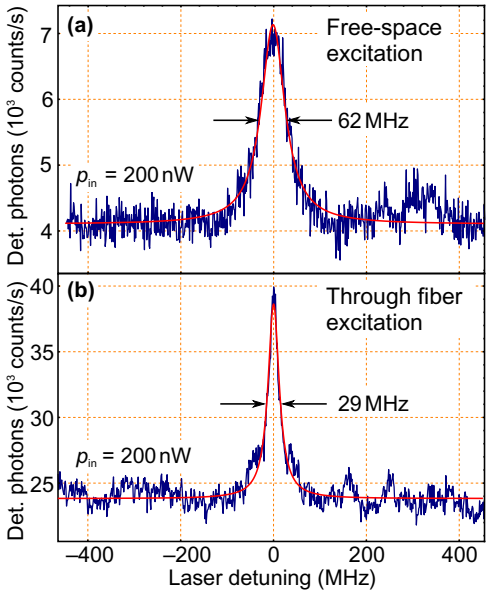

FIG. 4. Excitation lines of single molecules. (a) Fluorescence excitation spectrum of a single molecule under free-space excitation and fiber collection. (b) Spectral line of a single molecule under fiber excitation and detection.

The above experiments are conducted on many different DBATT molecules. Figure 5 shows an extended resonant excitation measurement in the fully fiber-coupled configuration. Each peak corresponds to a single molecule. The emission of the individual molecules resides on a constant level of background photons, which stem from the fiber. The heights of the peaks vary, as the coupling efficiency of the molecules is dependent on the position and orientation relative to the fiber core as outlined in the theory section above.

Each of the detected molecular lines can be further resolved by a finer frequency scan. Figure 5(b) shows an enlargement of the molecules in the upper panel (labeled), where the background emission of the fiber is subtracted. The included fit shows a typical Lorentzian behavior and displays a linewidth clearly below 100 MHz as in earlier studies [18,19,28]. The curve is fitted as

$$I_{\mathrm{out}}(\omega) \propto \frac{1}{(\omega-\omega_0)^2+\Gamma_2^2}\,, \tag{1}$$

where ω_0 denotes the angular frequency of the transition, ω the angular laser frequency, and Γ_2 the linewidth of the emitter.

As the molecules are long-time stable and there is no limitation by photobleaching under cryogenic conditions, it is possible to record long measurements at high excitation powers, as shown in Fig. 5(c), where we present a long-term (10 min) saturation scan. It is evident that the linewidth as well as its amplitude increases along with

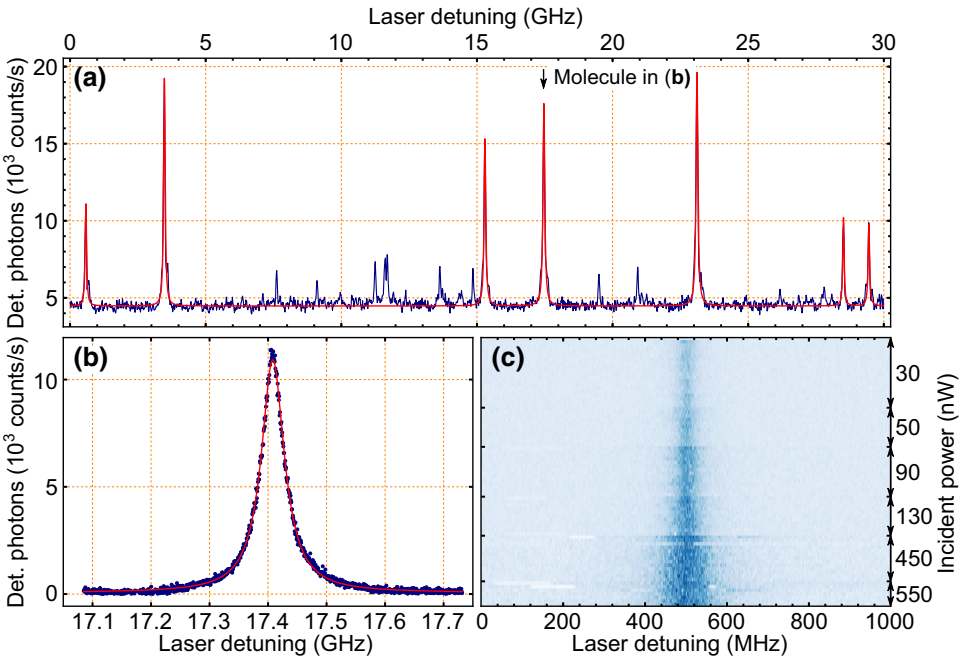

FIG. 5. Resonant excitation of molecules through the fiber. (a) Fluorescence-excitation spectrum of single molecules excited through the optical fiber with an input power of 50 nW. (b) Enlargement of one of the molecules of the spectrum in (a). With subtracted background the curve can be approximated with a pure Lorentzian. (c) A saturation scan where the molecule's line is recorded at different excitation powers.

excitation power. This is performed to record a saturation scan, which allows determination of the photophysical parameters.

The saturation scan not only reveals the achievable peak count rates, but is also an indication on the efficiency of the emitters' excitation. The background corrected saturation scan is shown in Fig. 6(a), where the emission count rate is plotted against the logarithmic incident power into the fiber. Saturation occurs at 60 nW, which exceeds the typical values obtained for the DBATT molecule with a focused laser by a factor of 10–100 [31]. The curve is fitted with the equation

$$I_{\text{out}}(I_{\text{in}}) = R_{\infty}\frac{I_{\text{in}}}{I_{\text{sat}} + I_{\text{in}}}, \tag{2}$$

where I_{out} is the number of emitted photons, I_{in} is the excitation intensity, I_{sat} is the saturation intensity, and R_{∞} is the extrapolated count rate at infinite excitation power.

The saturation count rate of around 50×10^3 counts/s is 10–25 times lower than the achievable count rates in confocal microscopy with a solid immersion lens [18,31]. We attribute this to the reduced coupling efficiency into the fiber, which is discussed in the theory section (factor 4 to 5). Furthermore, it is influenced by the reduced spectral contribution with a factor of around 3 to 4. To this end, the count rates are comparable for the DBATT molecule. With the present background contribution and the still limited NA of the fiber, we believe that the count rates will not be significantly higher until those constraints are addressed.

While the counts of the emitter are saturating, the spectral linewidth in the saturation scan also rises. This is described by the square-root proportionality, written as

$$\Delta\nu(I_{\text{in}}) = \frac{\Gamma_2}{\pi}\sqrt{1 + \frac{I_{\text{in}}}{I_{\text{sat}}}}, \tag{3}$$

where the linewidth at the low excitation limit is given as Γ_2/π and the incident intensity as I_{in}. For this particular molecule a minimum linewidth of 28.5 MHz is

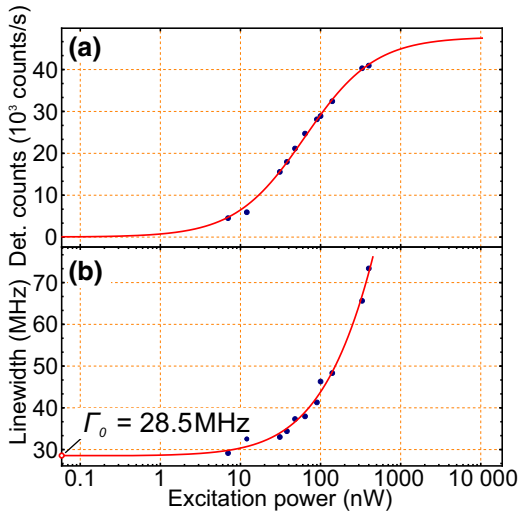

FIG. 6. Saturation and linewidth. (a) Saturation curve of the observed molecule. The behavior corresponds to the usual two-level system-broadening behavior. To note: the background of the fiber and impurities is subtracted in this scan. (b) Fitted linewidth of the molecule under increased excitation intensity. This curve allows the determination of the natural linewidth, which corresponds to the low-power limit.

found. This is larger than the typical values (see, e.g., Ref. [19]) by a factor of approximately 2. We attribute this to eventually opened relaxation channels due to the nearby interface, which may lead to cracks and strain in the formed Shpol'skiĭ-matrix. Over the course of these experiments, no narrower molecules are observed.

A crucial value for single-photon sources is the measurement of their photon autocorrelation function, $g^{(2)}(\tau)$. A measurement of $g^{(2)}(0) < 1$ proves a nonclassical behavior of the detected photon stream. A further reduced value of $g^{(2)}(0) < \frac{1}{2}$ indicates that we are typically dealing with single emitters [32]. Figure 7 shows the photon antibunching for the presented single-photon source. The measurement is performed at an excitation power of 350 nW, and results in an uncorrected $g^{(2)}(0) = 0.35 \pm 0.05$. Together with the measured molecule signal of 40×10^3 counts/s, and a background of 10×10^3 counts this value can be corrected to $g^{(2)}(0) = 0.01^{+0.05}_{-0.01}$ [see, e.g., [33], Supplement, Eq. (1)]. Subsequently, the source can be regarded as a genuine single-photon source.

Additionally, the molecules' autocorrelation curve shows coherent oscillations between the ground and the excited state, so-called Rabi oscillations [27,31,34]. To fit the curve in Fig. 7 we use

$$g^{(2)}(\tau) = 1 - \left[\cos\left(\Omega_{\text{Rabi}}|\tau|\right) + \frac{\Gamma_1 + \Gamma_2}{2\Omega_{\text{Rabi}}}\sin\left(\Omega_{\text{Rabi}}|\tau|\right)\right] \times e^{-\frac{(\Gamma_1+\Gamma_2)}{2}|\tau|}, \tag{4}$$

and introduce an additional background term [33]. $\Gamma_1 = 1/T_1$ denotes the longitudinal, and $\Gamma_2 = 1/T_2$ the transversal relaxation rate.

A ratio of $\Gamma_1/\Gamma_2 = 2$ indicates the Fourier-limited linewidth of the emitter. Since no independent measure of T_1 is available of this molecule, we cannot claim the strictly Fourier-limited nature of the single molecule's emission. As commonly observed, coherent Rabi oscillations further indicate that the molecule is driven above saturation.

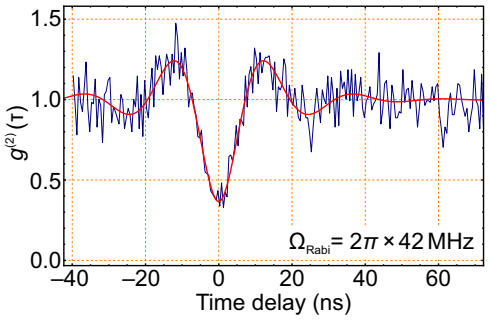

FIG. 7. Antibunching and Rabi oscillations. The single-photon stream is characterized by the photon antibunching value for $g^{(2)}(0)$, which is below the value of 0.5 without background correction. Coherent oscillations between the ground and excited state can be seen. The Rabi frequency is $\Omega_{\text{Rabi}} = 2\pi \times 42\,\text{MHz}$. Under the assumption of a lifetime-limited linewidth of $2\pi \times 28.5\,\text{MHz}$, we can fit this antibunching curve with a corresponding T_1 time of 14.6 ns.

V. CONCLUSION & OUTLOOK

In conclusion, we present a fiber-integrated single-photon source based on single DBATT molecules. By a change of the excitation scheme, the source is capable of emitting on the sodium D-line transitions [19]. The approach used to build the source is very general and can be applied to different molecules or even completely different emitters. Subsequently, a change of wavelength is straightforward. For example, it is possible to use the molecule dibenzoterrylene (DBT) in order to reach the atomic rubidium or potassium transitions [18]. Considering that Raman scattering scales with the fourth power against the wavelength, this reduces the Raman scattering in the fiber by a factor of 3. In the current implementation, the collection efficiency of the source is limited by spectral filtering and the presence of the high refractive index *n*-tetradecane in which the molecules are hosted. Therefore, to further increase the efficiency, a shorter fiber or one with less background can be employed, which relaxes the need for spectral filtering of the Raman contribution. In additional experiments, we analyze the option to use few-ns optical excitation pulses and time filtering for the molecular emission. When an optical pulse enters the optical fiber the Raman background is generated immediately; since the molecule is located only at the end of the fiber, a time window around the molecular emission allows reduction of the earlier generated background to negligible values, while also providing a triggered single-photon emission. As an alternative, a resonant excitation scheme can be implemented, such that the molecules are excited on their zero-phonon line, and the detection is realized in another polarization mode at the same wavelength. This allows us to circumvent the red-shifted Raman emission for single-photon detection. Additionally, it is possible to remove the high refractive index *n*-tetradecane solution, e.g., by placing a thin sublimated crystal, hosting the molecules on the fiber end facet [35,36].

The reported source can be a resource for quantum technologies and reduces the experimental complexity of cryogenic single molecule studies. We expect that a fully fiber-integrated source like the one presented here can be immediately used in applications such as quantum sensing and quantum key distribution.

ACKNOWLEDGMENTS

We acknowledge funding from the Deutsche Forschungsgemeinschaft in the project GE2737/5-1, the Max Planck Society, and the COST Action MP1403

"Nanoscale Quantum Optics" funded by COST (European Cooperation in Science and Technology). We also acknowledge discussions with Dr. Bert Hecht, Würzburg. We thank Dr. Jörg Wrachtrup for continuous support.

[1] M. Orrit and J. Bernard, Single Pentacene Molecules Detected by Fluorescence Excitation in a P-Terphenyl Crystal, Phys. Rev. Lett. **65**, 2716 (1990).

[2] Tim Schröder, Andreas W. Schell, Günter Kewes, Thomas Aichele, and Oliver Benson, Fiber-integrated diamond-based single photon source, Nano Lett. **11**, 198 (2011).

[3] Davide Cadeddu, Jean Teissier, Floris R. Braakman, Niels Gregersen, Petr Stepanov, Jean-Michel Gérard, Julien Claudon, Richard J. Warburton, Martino Poggio, and Mathieu Munsch, A fiber-coupled quantum-dot on a photonic tip, Appl. Phys. Lett. **108**, 011112 (2016).

[4] Ramachandrarao Yalla, Fam Le Kien, M. Morinaga, and K. Hakuta, Efficient Channeling of Fluorescence Photons from Single Quantum Dots Into Guided Modes of Optical Nanofiber, Phys. Rev. Lett. **109**, 063602 (2012).

[5] Masazumi Fujiwara, Kiyota Toubaru, Tetsuya Noda, Hong-Quan Zhao, and Shigeki Takeuchi, Highly efficient coupling of photons from nanoemitters into single-mode optical fibers, Nano Lett. **11**, 4362 (2011).

[6] Andreas W. Schell, Hideaki Takashima, Shunya Kamioka, Yasuko Oe Masazumi Fujiwara, Oliver Benson, and Shigeki Takeuchi, Highly efficient coupling of nanolight emitters to a ultra-wide tunable nanofibre cavity, Sci. Rep. **5**, 9619 (2015).

[7] Alexander Schlehahn, Sarah Fischbach, Ronny Schmidt, Arsenty Kaganskiy, Andre Strittmatter, Sven Rodt, Tobias Heindel, and Stephan Reitzenstein, A stand-alone fiber-coupled single-photon source, Sci. Rep. **8**, 1340 (2018).

[8] Lars Liebermeister, Fabian Petersen, Asmus v Münchow, Daniel Burchardt, Juliane Hermelbracht, Toshiyuki Tashima, Andreas W. Schell, Oliver Benson, Thomas Meinhardt, and Anke Krueger *et al.*, Tapered fiber coupling of single photons emitted by a deterministically positioned single nitrogen vacancy center, Appl. Phys. Lett. **104**, 031101 (2014).

[9] Vadim V. Vorobyov, Vladimir V. Soshenko, Stepan V. Bolshedvorskii, Javid Javadzade, Nikolay Lebedev, Andrey N. Smolyaninov, Vadim N. Sorokin, and Alexey V. Akimov, Coupling of single nv center to adiabatically tapered opticalsingle mode fiber, Eur. Phys. J. D **70**, 269 (2016).

[10] Masazumi Fujiwara, Oliver Neitzke, Tim Schröder, Andreas W. Schell, Janik Wolters, Jiabao Zheng, Sara Mouradian, Mohamed Almoktar, Shigeki Takeuchi, and Dirk Englund *et al.*, Fiber-coupled diamond microwaveguides toward an efficient quantum interface for spin defect centers, ACS Omega **2**, 7194 (2017).

[11] Andreas W. Schell, Hideaki Takashima, Toan Trong Tran, Igor Aharonovich, and Shigeki Takeuchi, Coupling quantum emitters in 2D materials with tapered fibers, ACS Photonics **4**, 761 (2017).

[12] Sarah M. Skoff, David Papencordt, Hardy Schauffert, Bernhard C. Bayer, and Arno Rauschenbeutel, Optical-nanofiber-based interface for single molecules, Phys. Rev. A **97**, 043839 (2018).

[13] Sanli Faez, Pierre Türschmann, Harald R. Haakh, Stephan Götzinger, and Vahid Sandoghdar, Coherent Interaction of Light and Single Molecules in a Dielectric Nanoguide, Phys. Rev. Lett. **113**, 213601 (2014).

[14] Sanli Faez, Yoav Lahini, Stefan Weidlich, Rees F. Garmann, Katrin Wondraczek, Matthias Zeisberger, Markus A. Schmidt, Michel Orrit, and Vinothan N. Manoharan, Fast, label-free tracking of single viruses and weakly scattering nanoparticles in a nanofluidic optical fiber, ACS Nano **9**, 12349 (2015).

[15] Günter Kewes, Max Schoengen, Oliver Neitzke, Pietro Lombardi, Rolf-Simon Schönfeld, Giacomo Mazzamuto, Andreas W. Schell, Jürgen Probst, Janik Wolters, and Bernd Löchel *et al.*, A realistic fabrication and design concept for quantum gates based on single emitters integrated in plasmonic-dielectric waveguide structures, Sci. Rep. **6**, 28877 (2016).

[16] P. Lombardi, A. P. Ovvyan, S. Pazzagli, G. Mazzamuto, G. Kewes, O. Neitzke, N. Gruhler, O. Benson, W. H. P. Pernice, and F. S. Cataliotti *et al.*, Photostable molecules on chip: Integrated sources of nonclassical light, ACS Photonics **5**, 126 (2017).

[17] Pierre Türschmann, Hanna Le Jeannic, Signe F. Simonsen, Harald R. Haakh, Stephan Götzinger, Vahid Sandoghdar, Peter Lodahl, and Nir Rotenberg, Coherent nonlinear optics of quantum emitters in nanophotonic waveguides, Nanophotonics **8**, 1641 (2019).

[18] Petr Siyushev, Guilherme Stein, Jörg Wrachtrup, and Ilja Gerhardt, Molecular photons interfaced with alkali atoms, Nature **509**, 66 (2014).

[19] Wilhelm Kiefer, Mohammad Rezai, Jörg Wrachtrup, and Ilja Gerhardt, An atomic spectrum recorded with a single molecule light source, Appl. Phys. B: Lasers Opt. **122**, 1 (2016).

[20] Eric R. I. Abraham and Eric A. Cornell, Teflon feedthrough for coupling optical fibers into ultrahigh vacuum systems, Appl. Opt. **37**, 1762 (1998).

[21] Patrick Then, Gary Razinskas, Thorsten Feichtner, Philippe Haas, Andreas Wild, Nicola Bellini, Roberto Osellame, Giulio Cerullo, and Bert Hecht, Remote detection of single emitters via optical waveguides, Phys. Rev. A **89**, 053801 (2014).

[22] Navid Soltani and Mario Agio, Planar antenna designs for efficient coupling between a single emitter and an optical fiber, Opt. Express **27**, 30830 (2019).

[23] Yusuke Morisawa, Shin Tachibana, Akifumi Ikehata, Tao Yang, Masahiro Ehara, and Yukihiro Ozaki, Changes in the electronic states of low-temperature solid *n*-tetradecane: Decrease in the homo-lumo gap, ACS Omega **2**, 618 (2017).

[24] W. Lukosz, Light emission by magnetic and electric dipoles close to a plane dielectric interface. III. Radiation patterns of dipoles with arbitrary orientation, J. Opt. Soc. Am. **69**, 1495 (1979).

[25] Mohammad Rezai, Jörg Wrachtrup, and Ilja Gerhardt, Coherence Properties of Molecular Single Photons for

Quantum Networks, Phys. Rev. X **8**, 031026 (2018).

[26] K. G. Lee, X. W. Chen, H. Eghlidi, P. Kukura, R. Lettow, A. Renn, V. Sandoghdar, and S. Götzinger, A planar dielectric antenna for directional single-photon emission and near-unity collection efficiency, Nat. Photonics **5**, 166 (2011).

[27] Mohammad Rezai, Jörg Wrachtrup, and Ilja Gerhardt, Detuning dependent Rabi oscillations of a single molecule, New J. Phys. **21**, (2019).

[28] A. M. Boiron, B. Lounis, and M. Orrit, Single molecules of dibenzanthanthrene in *n*-hexadecane, J. Chem. Phys. **105**, 3969 (1996).

[29] Wilhelm Kiefer, Robert Löw, Jörg Wrachtrup, and Ilja Gerhardt, Na-Faraday rotation filtering: The optimal point, Sci. Rep. **4**, 6552 (2014).

[30] Ilja Gerhardt, How anomalous is my Faraday filter? Opt. Lett. **43**, 5295 (2018).

[31] G. Wrigge, I. Gerhardt, J. Hwang, G. Zumofen, and V. Sandoghdar, Efficient coupling of photons to a single molecule and the observation of its resonance fluorescence, Nat. Phys. **4**, 60 (2008).

[32] Mohammad Rezai, Jan Sperling, and Ilja Gerhardt, What can single photons do what lasers cannot do? Quantum Sci. Technol. **4**, 1 (2019).

[33] Andreas W. Schell, Johannes Kaschke, Joachim Fischer, Rico Henze, Janik Wolters, Martin Wegener, and Oliver Benson, Three-dimensional quantum photonic elements based on single nitrogen vacancy-centres in laser-written microstructures, Sci. Rep. **3**, 1577 (2013).

[34] Samuele Grandi, Kyle D. Major, Claudio Polisseni, Sebastien Boissier, Alex S. Clark, and E. A. Hinds, Quantum dynamics of a driven two-level molecule with variable dephasing, Phys. Rev. A **94**, 063839 (2016).

[35] R. J. Pfab, J. Zimmermann, C. Hettich, I. Gerhardt, A. Renn, and V. Sandoghdar, Aligned terrylene molecules in a spin-coated ultrathin crystalline film of *p*-terphenyl, Chem. Phys. Lett. **387**, 490 (2004).

[36] Claudio Polisseni, Kyle D. Major, Sebastien Boissier, Samuele Grandi, Alex S. Clark, and E. A. Hinds, Stable, single-photon emitter in a thin organic crystal for application to quantum-photonic devices, Opt. Express **24**, 5615 (2016).